sustainability

MDPI

Article

A Novel Joint Time-Frequency Spectrum Resources Sustainable Risk Prediction Algorithm Based on TFBRL Network for the Electromagnetic Environment

Shuang Li [1], Yaxiu Sun [1], Yu Han [1,*], Osama Alfarraj [2], Amr Tolba [2] and Pradip Kumar Sharma [3]

[1] College of Information and Communication Engineering, Harbin Engineering University, Harbin 150001, China
[2] Computer Science Department, Community College, King Saud University, Riyadh 11437, Saudi Arabia
[3] Department of Computing Science, University of Aberdeen, Aberdeen AB24 3FX, UK
* Correspondence: yu.han1001@hrbeu.edu.cn

Abstract: To protect the electromagnetic environment and understand its current state in a timely manner, monitoring the electromagnetic environment has great practical significance, while massive amounts of data are generated. It is crucial to utilize data mining technology to extract valuable information from these massive amounts of data for effective spectrum management. Traditional spectrum prediction methods do not integrate the prior information of spectrum resource occupancy, so that the prediction of the channel state of a single frequency point is of limited significance. To address these issues, the paper describes a dynamic threshold algorithm which mines bottom noise and spectrum resource occupancy from massive electromagnetic environment data. Moreover, the paper describes a joint time-frequency spectrum resource prediction algorithm based on the time-frequency block residual LSTM (TFBRL) network, which utilizes hourly time closeness, daily period, and annual trend as prior knowledge of spectrum resources. The TFBRL network comprises three main parts: (1) a residual convolution network with a squeeze-and-excitation (SE) attention mechanism, (2) a long short term memory (LSTM) model with memory ability to capture sequence latent information, and (3) a feature fusion module based on a matrix to combine time closeness, daily period, and annual trend feature components. Experimental results demonstrate that the TFBRL network outperforms the baseline networks, improving by 31.37%, 16.00% and 13.06% compared with the best baseline for MSE, RMSE and MAE, respectively. Thus, the TFBRL network has good risk prediction performance and lays the foundation for subsequent frequency scheduling.

Keywords: big data mining; spectrum prediction; TFBRL network; deep learning

Citation: Li, S.; Sun, Y.; Han, Y.; Alfarraj, O.; Tolba, A.; Sharma, P.K. A Novel Joint Time-Frequency Spectrum Resources Sustainable Risk Prediction Algorithm Based on TFBRL Network for the Electromagnetic Environment. *Sustainability* **2023**, *15*, 4777. https://doi.org/10.3390/su15064777

Academic Editor: Andreas Kanavos

Received: 31 December 2022
Revised: 21 February 2023
Accepted: 2 March 2023
Published: 8 March 2023

1. Introduction

Human civilization has progressed scientifically and technologically in recent years, and the development process of computer technology has also accelerated, including automatic modulation classification technology [1–4] in the field of communication, federated learning technology for information privacy and security [5], complex electromagnetic environment portrait technology [6], ADS-B (Automatic dependent surveillance-broadcast) target recognition technology [7], information countermeasure attack and defense technology [8,9], complex electromagnetic environment visualization technology [10] and transfer learning technology [11], etc. These computer science research results in turn further drive the progress of human society and technology [12]. In this process, big data records important information of various industries, which provides important information for risk assessment and prediction as well as power allocation [13].

Big data mining technology based on mathematical, physical, and artificial intelligence models has a significant impact in many areas. For instance, [14] developed a three-parameter correlation model considering the chemical characteristics of a sample

and the experimental operating circumstances to forecast the mass heat capacity for biomaterials. The authors of [15] explored the interplay between interparticle attraction and hydrodynamic stresses to elucidate the physical foundations of colloidal gel rheology. In [16], the author used different features of the approximate signal and extracted component information of the signal to perform flow classification and voidage prediction, which greatly strengthens system performance prediction in the industrial sector.

In the monitoring process of the complex electromagnetic environment, with the increase of monitoring time, massive amounts of electromagnetic environment big data can be collected and stored [17]. The value carried by electromagnetic environment big data information is sparse, and big data mining technology is needed to convert big data into big insights. Currently the research on electromagnetic environment big data is evolving, and several new big data mining and analysis methods have been introduced to this field, including machine learning methods, to improve on the disadvantages of traditional methods, given the mining method's ability to predict and attain more complex insights, such as spectrum resources sustainable risk prediction.

The restricted spectrum resources are currently scarce and congested due to the quick expansion of numerous devices that use different frequencies [18]. In the original static spectrum allocation strategy, the main user occupying a specific frequency band to work will cause a spectrum hole [19], that is, the waste and inefficiency of spectrum resources, which will lead to an increase in the sustainable risk of spectrum resources. A schematic diagram of spectrum holes is shown in Figure 1. If the occurrence of spectrum holes can be sensed and the activities of secondary users can be scheduled to the places where the spectrum holes are located, it is possible to increase the usage of spectrum resources, more users can work in an orderly and efficient manner within a limited spectrum range, and the spectrum resources sustainable risk will be reduced. Spectrum prediction technology can effectively predict the sustainable risk of spectrum resources. Therefore, the study of spectrum prediction technology is of great practical significance.

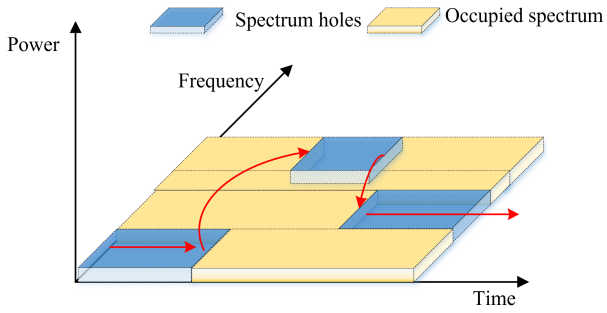

Figure 1. Schematic diagram of spectrum holes.

In the process of studying the complex electromagnetic environment, the big data of the electromagnetic environment is first obtained through spectrum sensing [20], and then the relevant information such as the bottom noise and spectrum occupancy of the electromagnetic environment is obtained through a big data mining algorithm [21], and then stored in the spectrum state memory. Then, based on the historical data, a statistical regression model or the machine learning model which has emerged in recent years is used for learning and prediction. In this way, with the assistance of prediction information, spectrum sensing can lock a smaller electromagnetic environment spectrum monitoring range and achieve sustainable and efficient usage.

Currently, spectrum prediction technology is receiving growing research attention because of these benefits. In [22], the authors deduced a set of theories to analyze the predictability of real electromagnetic spectrum data, proving that the electromagnetic spectrum is predictable, which provides support for the achievability of subsequent electromagnetic spectrum prediction techniques. In early spectrum prediction technology, the AR (autoregressive) model [23], the SVR (support vector regression) model [24] and the hidden

markov-based model [25] received extensive attention and application. However, these classical models have certain limitations and are greatly affected by feature engineering. The authors of [26] established a characteristic function to model wireless signal strength in the mobile service band and realized low error prediction on real spectrum data.

With the rise of machine learning technology, MLP [27], RNN [28], and LSTM [29] have been extensively used in the area of spectrum prediction and obtained high prediction accuracy. Subsequently, the attention mechanism was applied to spectrum prediction and it can assign different weights to different frequency points and different time slots [30], achieving accurate spectrum prediction. The prediction of multi-frequency points has a greater application value than the spectrum prediction of single frequency points [31]. To further improve the performance of spectrum prediction, ref. [32] fused an external factor fusion module to the spectrum prediction network TF^{2}AN to model the weather and temperature characteristics of the spectrum. In [33], the rates of user blocking and waiting probability were reduced, and the spectrum utilization rate of CB-STSSN was enhanced. The MTF^{2}N constructed in [34] merged the CNN network and the LSTM network to achieve multi-channel and multi-slot spectrum prediction. To solve the problem of multiple training parameters and slow convergence of the machine learning model, the model-enabled autoregressive network [35] was proposed, and the model has both high frequency spectral predictability and fast model convergence speed.The authors of [36] constructed the electromagnetic spectrum graph neural network, which effectively reduced the spectrum prediction error of the multi-site.

As shown in the summary of the literature review in Table 1, there are few spectrum prediction technologies presented in the current literature which can simultaneously predict time-frequency two-dimensional spectrum occupancy, and most of the existing research directly analogizes the prediction of spectrum occupancy to the prediction of time series, thus paying no attention to the time closeness, period, and trend of spectrum occupancy, which make spectrum prediction lose a lot of prior information. Therefore, to overcome this disadvantage, this paper focuses on a study of time-frequency two-dimensional spectrum occupancy image prediction.

The following is a summary of this paper's major contributions.

- To obtain the sustainable risk information of the electromagnetic environment spectrum, this paper presents a dynamic threshold extraction algorithm for the bottom noise and occupancy of the electromagnetic environment spectrum. The dataset constructed in this paper integrates multiple features of electromagnetic environment spectrum data, such as time closeness, period, and trend, and adopts a matrix-based multi-feature fusion method to realize the mining of deep electromagnetic-spectrum-related information from a long-term time domain scale.
- This paper presents a model called TFBRL for spectrum prediction, which combines the characteristics of deep-level spectrum data mining of deep residual networks and the time series memory characteristics of the LSTM network, fully mining the image characteristics and time series characteristics of the electromagnetic spectrum. At the same time, this paper integrates the SE attention mechanism, and the designed network improves the accuracy of electromagnetic environment spectrum occupancy prediction, which can provide reliable materials for electromagnetic environment spectrum resource sustainability risk prediction.
- The real-world dataset from Turku is cleansed and analyzed comprehensively. This paper studies the two-dimensional image prediction of multiscale electromagnetic environment spectrum occupancy and builds spectrum occupancy image prediction network models under 20 spectrum image sizes with spectrum occupancy image sizes ranging from 4 to 44. To demonstrate TFBRL's superiority compared to five baselines, experiments are carried out. Then, the effectiveness of TFBRL is also verified on the dataset under various conditions.

The remaining portions of the paper are structured as follows: The big data mining method of the electromagnetic environment is introduced in Section 2, including the bottom

noise mining and spectrum occupancy mining based on an adaptive threshold. Section 3 introduces the TFBRL network designed in this paper for spectrum resource sustainability risk prediction, and introduces the generation of network input tensor data as well as the network structure and principles. The experimental findings and analysis of big data mining for the electromagnetic environment and risk projection for the sustainability of spectrum resources are presented in Section 4. The paper is concluded in Section 5.

Table 1. Summary table for the literature review.

Literature	Year	Methodology	Results
[23]	2008	Autoregressive (AR) model	AR model can greatly reduce the frequency conflict between users.
[24]	2009	Support vector regression (SVR) model	SVR model works better than other non-linear methods.
[25]	2018	Hidden markov-based model	Compared with the spectrum prediction based on local and hard fusion, the model effectively reduced the spectrum prediction error.
[26]	2013	Statistical model	The statistical model significantly improved the long-term average achievable throughput.
[27]	2010	Multilayer perceptron (MLP)	MLP can achieve good prediction performance without prior knowledge.
[28]	2013	Recurrent neural network (RNN)	The model had less error prediction probability in spectrum occupancy state prediction.
[29]	2017	Long short term memory (LSTM)	The LSTM network had great and robust prediction performance.
[32]	2021	Temporal-frequency fusion attention network (TF^2AN)	This structure showed considerable effectiveness for spectrum prediction with sufficient data.
[33]	2021	Cloud-based satellite and terrestrial spectrum shared networks (CB-STSSN)	The rate of user blocking and waiting probability were reduced, and the spectrum utilization rate of CB-STSSN was enhanced.
[34]	2022	Multi-channel temporal-frequency fusion network (MTF^2N)	The MTF^2N outperformed LSTM, Seq2seq, and GRU networks in terms of accuracy in the long-term spectrum forecast.
[35]	2022	Model-enabled autoregressive network	The model had both high frequency spectral predictability and fast model convergence speed.
[36]	2023	Graph convolution network	The model effectively reduced the spectrum prediction error of the multi-site.
This work	2023	Time-frequency block residual lstm (TFBRL)	The TFBRL network outperformed the baseline networks, with an average improvement of 31.37%, 16.00%, and 13.06% over the best baseline of MSE, RMSE, and MAE, respectively.

2. Electromagnetic Environment Big Data Mining

2.1. System Model

Due to the growing scarcity of radio spectrum resources and the low efficiency of the currently available spectrum resources, allocating spectrum resources dynamically in accordance with real-time spectrum utilization to optimize spectrum utilization efficiency has become a focus of research. Figure 2 shows the system for spectrum data mining and prediction considered in the paper. In this complex electromagnetic environment monitoring, firstly, various kinds of electromagnetic environment monitoring equipment deployed in the real electromagnetic environment collect electromagnetic spectrum data, and then the electromagnetic environment big data mining algorithm will be used to analyze valuable information such as electromagnetic environment noise and spectrum

occupancy. In order to predict the risk of frequency spectrum sustainability, this paper designs a TFBRL network model to model and predict the electromagnetic spectrum occupancy obtained by big data mining, which provides knowledge guidance for secondary users to dynamically access the idle spectrum, so as to promote the sustainable utilization and utilization rate of the electromagnetic spectrum.

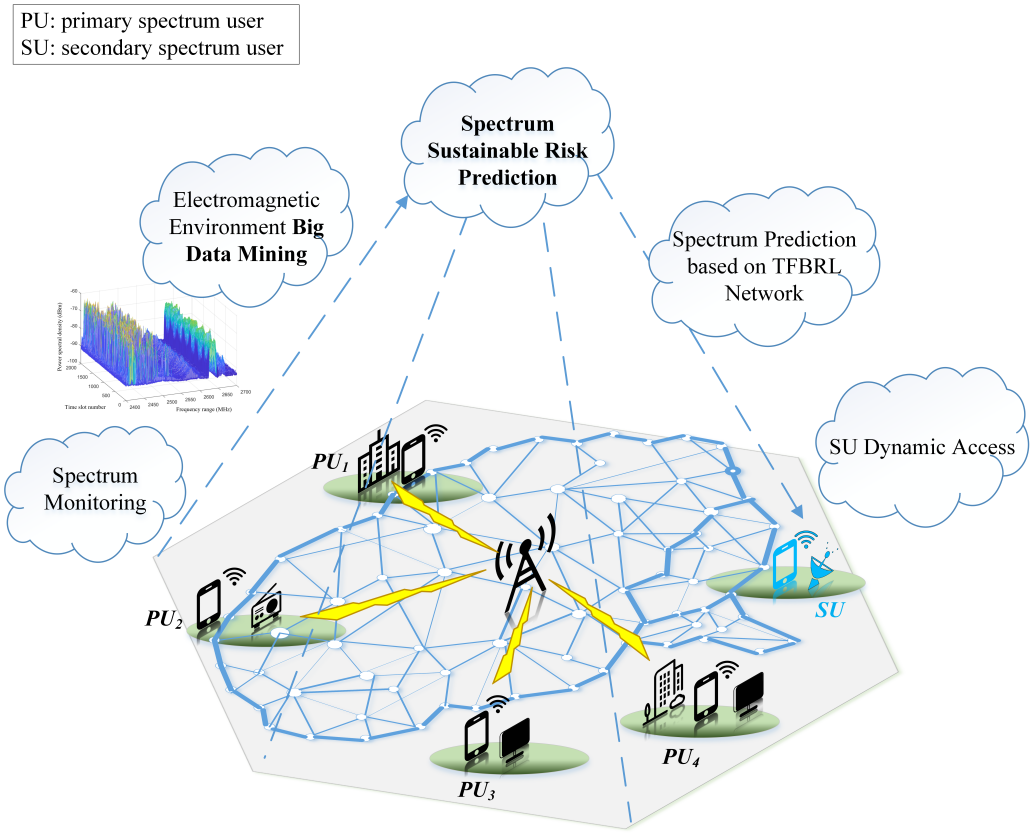

Figure 2. System for spectrum data mining and prediction.

2.2. Mining of Electromagnetic Environmental Noise

When performing spectrum monitoring, it is assumed that the deployed spectrum monitoring equipment can simultaneously obtain the spectrum monitoring data of adjacent n frequency points at a certain time. During m monitoring timeslots, $m \times n$ power spectral density values can be obtained, which can be expressed as Equation (1).

$$\mathbb{S} = (\mathbb{S}_1, \mathbb{S}_2, \mathbb{S}_3, \mathbb{S}_4, \ldots, \mathbb{S}_n), \mathbb{S} \in R^{m \times n} \quad (1)$$

Here, m refers to the monitoring time, totaling m time slots; n is the amount of frequency points. The power spectrum value vector obtained by channel number 1 in m time slots is denoted by $\mathbb{S}_1$.

Before determining the channel occupancy state threshold $\mathbb{S}_{i,j}^t$, electromagnetic environment noise needs to be determined. For electromagnetic environment noise mining, this paper uses a variety of signal processing algorithms to analyze and mine noise evolution trends. The bottom noise mining process is shown in Figure 3.

Bottom noise data is one of the most important data in electromagnetic spectrum big data mining. The channel with high bottom noise is not conducive to signal transmission, while the channel with low bottom noise is conducive to signal transmission. The key problem in the bottom noise mining of the electromagnetic environment is the selection of a noise dynamic threshold. The dynamic threshold selection of bottom noise mainly serves to divide the original data into threshold values. First, the data with signal and the data

without signal can be separated. Data without signal are regarded as the original bottom noise data, while data with signal are regarded as a mixture of bottom noise and signal.

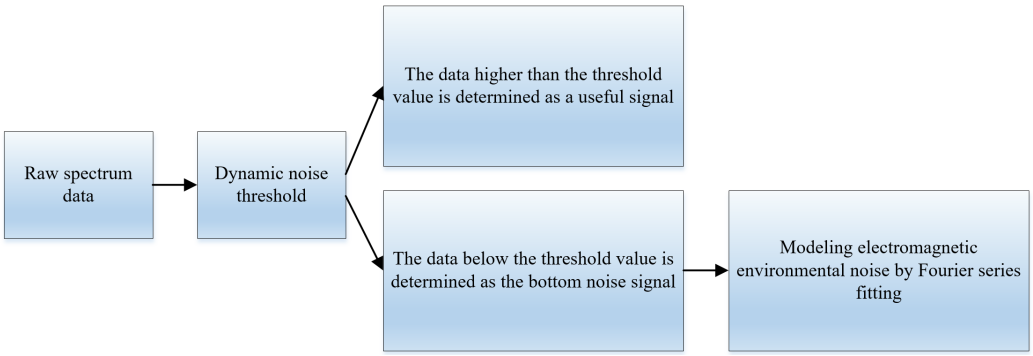

Figure 3. Bottom noise mining in the electromagnetic environment.

In this paper, a calculation method based on adaptive dynamic thresholds is used to mine the bottom noise data. Because the corresponding services of different frequency bands are different, this paper calculates different dynamic noise thresholds for different frequency points. Algorithm 1 introduces the calculation method for dynamic noise thresholds in the electromagnetic environment in detail. The calculation formula for the electromagnetic environment bottom noise threshold T is presented in Equation (2).

$$T = \frac{1}{nk}\sum_{j=1}^{nk} M(j) + (F_{\max} - F_{\min}) * k_2 \tag{2}$$

where nk is the number of lines with k_1 ratio in raw spectrum data lines, after sorting the spectrum data. $M(j)$ is the sum of the energy of the reserved lines, k_2 is the weight of the range of the energy data, and $F_{\max}$ and $F_{\min}$ represent the maximum and minimum energy.

Algorithm 1 Dynamic threshold value of bottom noise

Input: Frequency domain sample set $\mathbb{S} = (\mathbb{S}_1, \mathbb{S}_2, \mathbb{S}_3, \mathbb{S}_4, \ldots, \mathbb{S}_n), \mathbb{S} \in R^{m \times n}$, weight k_1 and k_2.

Output: Dynamic threshold value of bottom noise $T = (T_1, T_2, T_3, T_4, \ldots, T_n), T \in R^{1 \times n}$

1: **for** $\mathbb{S}_f\left(\mathbb{S}_f \in R^{m \times 1}, f \in [1:n]\right)$ *in Frequency domain sample set X* **do**
2: Sort spectrum data $\mathbb{S}_{i,j}$ in $\mathbb{S}_f$ in ascending order;
3: Take the spectrum value $\mathbb{S}_{i,j}$ of the bottom $k_1 (k_1 \in [0,1])$ after sorting, and record it as set M;
4: Define $a_f = \sum_{j=1}^{nk} \frac{M_j}{nk}$, $nk = \text{int}(m \times k_1), j = 1, 2, 3, \ldots, nk$;
5: Calculate the range of the sample $S_f = \max(\mathbb{S}_{i,j}) - \min(\mathbb{S}_{i,j})$;
6: Dynamic threshold value of bottom noise is $T_i = a_f + k_2 \times S_f$.
7: **return** Dynamic threshold $T = (T_1, T_2, T_3, T_4, \ldots, T_n)$

The data below the threshold are fitted as the bottom noise after determining the dynamic noise threshold of the electromagnetic environment. The fitting model selected in this paper is the Fourier series, which has good fitting effect and short fitting operation time. Therefore, the unified expression of electromagnetic environmental noise based on the Fourier series obtained in this paper is shown in Equation (3).

$$F(\rho) = C_0 + \sum_{j=1}^{n} \xi_j * \cos(j * \rho * w) + \sum_{j=1}^{n} \zeta_j * \sin(j * \rho * w) \tag{3}$$

Here, C_0, ξ_j and ζ_j are constant.

2.3. Mining of Electromagnetic Environmental Spectrum Occupancy

The spectrum usage is measured by calculating the spectrum occupancy. After modeling the electromagnetic environment bottom noise, the bottom noise value of any time slot and any frequency point can be determined. The dynamic threshold of spectrum occupancy is the bottom noise value plus 3dB, which is shown in Equation (4)

$$\mathbb{S}_{i,j}^{t} = \mathbb{S}_{i,j}^{nt} + 3dB \tag{4}$$

where $\mathbb{S}_{i,j}^{nt}$ denotes the electromagnetic environmental bottom noise and $\mathbb{S}_{i,j}^{t}$ denotes the dynamic threshold of spectrum occupancy. Then according to the following formula, discrete mapping can be performed.

$$x_{i,j} = \begin{cases} 1, & \text{when } \mathbb{S}_{i,j} > \mathbb{S}_{i,j}^{t} \\ 0, & \text{when } x_{i,j} \leq \mathbb{S}_{i,j}^{t} \end{cases} \tag{5}$$

where $\mathbb{S}_{i,j}$ refers to power spectral density value and $x_{i,j}$ represents the channel occupancy state.

Then the spectrum occupancy SO is the ratio in Equation (6). Here, T_0 is the duration that the spectrum power spectral density value is higher than the spectrum occupancy state threshold, and T_T is the total monitoring duration.

$$SO = \frac{T_0}{T_T} \tag{6}$$

3. Prediction of Spectrum Resource Sustainability Risk Based on TFBRL Network

The sustainability risk of spectrum resources is closely related to the spectrum occupancy of current spectrum resources. For spectrum resources with high spectrum occupancy, frequency planning will become more crowded, and interference or conflict between different frequency using devices will easily occur, which will reduce the sustainability of spectrum resources and increase the sustainability risk. On the contrary, for a frequency band with low spectrum occupancy, frequency planning is less and is generally idle, so the sustainability risk of spectrum resources is low. Therefore, spectrum occupancy can be used as an important indicator to reflect the sustainability risk of spectrum resources.

In the second section, this paper reported data mining on the real electromagnetic environment big data and obtained the mining information such as spectrum occupancy. Here, the electromagnetic spectrum occupancy data obtained from the mining is processed into a spectrum occupancy time-frequency block, which is composed of m time slots and n frequency points. The acquisition diagram of each time-frequency block is shown in Figure 4. Three multi-scale sliding windows are adopted to obtain the spectrum occupancy image in the time and frequency domain, and multi-scale time-frequency block data are constructed in the form of multidimensional tensors. In the process of multi-scale time-frequency block construction, each time-frequency block tensor is composed of three dimensions: one is the data of adjacent past time to simulate closeness, the other is the data of the same period of the previous day to simulate period, and the third is the data of the same time period of the previous year to simulate trend and to jointly predict time-frequency spectrum occupancy image blocks. The generation steps of the time-frequency block is displayed in Figure 4.

The TFBRL network is comprised of three important components modeling time-frequency closeness, period and trend. The architecture of the TFBRL network is presented in Figure 5.

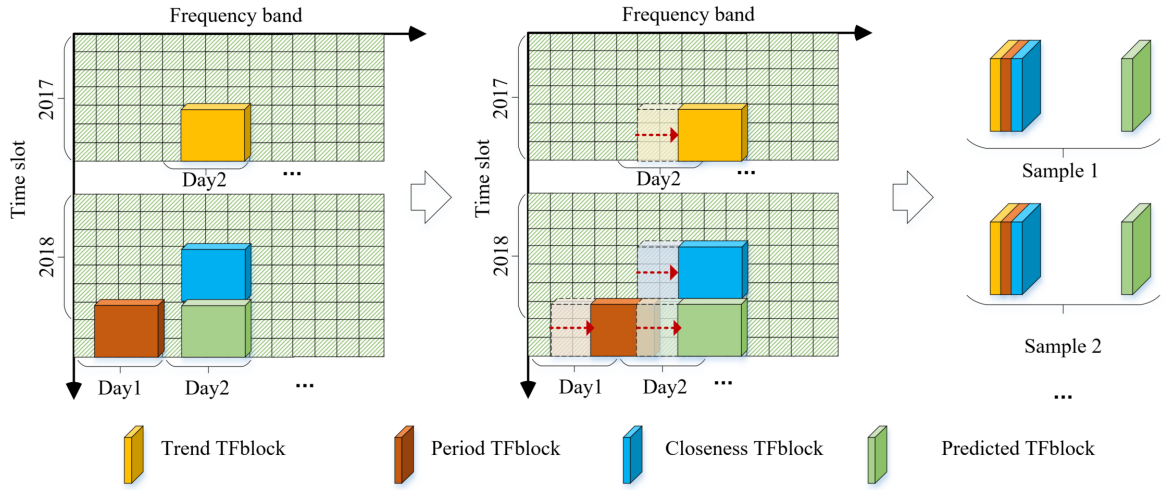

Figure 4. Construction process of time-frequency block data. TFblock: time-frequency block.

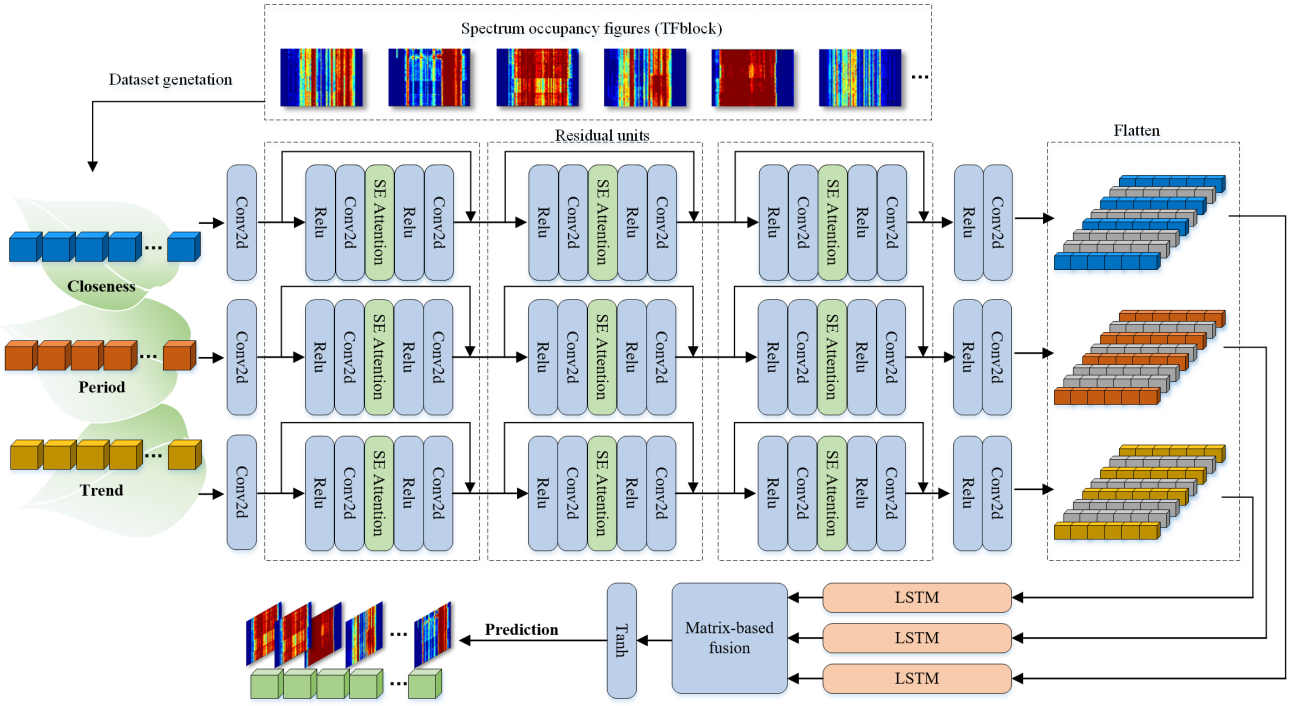

Figure 5. TFBRL architecture. Conv2d: Convolution; TFBRL: Time-frequency Block Resnet Lstm.

The main components of the network are convolutional residual network modules, with the SE attention mechanism, long short memory network module and matrix based fusion module. First, the convolutional neural network is introduced to extract latent features in the three types of time-frequency block data, and then residual modules are introduced to reduce the disappearance of features. Before being input into the LSTM network, the two-dimensional time-frequency features obtained from mining are flattened into one-dimensional features. The one-dimensional features use the memory characteristics of the LSTM network for time series to mine the feature information of time series. Finally, the matrix-based fusion module fuses various features from the three components with a matrix of different weights. The three main modules of TFBRL are introduced in the following.

3.1. Convolutional Residual Network Module with SE Attention Mechanism

1. Convolution. The spectrum occupancy data of the electromagnetic environment usually contains a large number of time slots and frequency point spectrum resource information. There will be an influence of and correlation between different frequency points and different time slots' spectrum resource information. This hidden correlation feature can be effectively extracted through a convolutional neural network. The convolutional neural network has a strong ability to capture the information of adjacent time and frequency points in time-frequency blocks. Since the spectrum resource information of different frequency points may have similar rules, this paper uses a multi-layer convolutional neural network to capture the dependence of non-adjacent frequency points. Suppose that the three time-frequency occupation image blocks used to model time closeness, period and trend are $X_c^i, X_p^i, X_t^i \in \mathbb{R}^{C\times H\times W}$ respectively. The closeness tensor data will have the following formula (7) after convolution:

$$X_c^{(m)} = \zeta\left(W_c^{(m)} * X_c^{(i)} + b_c^{(m)}\right) \tag{7}$$

where $*$ denotes the convolution; ζ is an activation function, e.g., the rectifier $\zeta(z) = max(0, z)$; and $W_c^{(m)}$ and $b_c^{(m)}$ are learnable parameters.

2. Residual Unit. Although the activation function is applied, the very deep convolution network will make the network training effect decline. To mine the spectrum resource information of electromagnetic environment big data, a relatively deep network is needed to capture the huge time-frequency dependency. Therefore, this work uses a residual learning network in the model. In the TFBRL network, residual units are stacked and a residual unit can be expressed through formula (8)

$$X_c^{(m+1)} = X_c^{(m)} + F\left(X_c^{(m)}; \theta_c^{(m)}\right) \tag{8}$$

where F is the residual function, and $\theta_c^{(m)}$ includes all learnable parameters in the mth residual unit.

3. SE Attention Module. This paper introduces the squeeze-and-excitation (SE) attention module, which aims to improve modeling ability by enabling the model to dynamically modulate the weight of each channel, thereby recalibrating the features. Squeeze and excitation are at the core of the SE attention mechanism. In Figure 6, the operation of the first box is squeeze. Specifically, it keeps the number of channels of the input feature unchanged, but interprets the size of the feature map of each channel as a set of local descriptors, and its statistics can express the entire image. The calculation process of squeeze is shown in Formula (9)

$$\eta = \mathbf{F}_{sq}(\aleph_c) = \frac{1}{H\times W}\sum_{i=1}^{H}\sum_{j=1}^{W}\aleph_c(i,j) \tag{9}$$

where $\aleph_c(i,j)$ are the network's characteristic values.
In Figure 6, The operation in the second box is excitation. The final output value is mapped to the range of 0–1. The calculation process of excitation is shown in Equation (10).

$$\delta = \mathbf{F}_{\text{ex}}(\eta, \mathbf{W}) = \sigma(g(\eta, \mathbf{W})) = \sigma(\mathbf{W}_2\delta(\mathbf{W}_1\eta)) \tag{10}$$

Here, the vector η obtained in the previous step is processed through two fully connected layers, W_1 and W_2, to obtain the desired channel weight value δ. After the two fully connected layers, different values in s represent the weight information of different channels, giving different weights to channels. The final operation is to multiply the calculated weight matrix and the input characteristic tensor, and assign the weight to the input characteristic tensor.

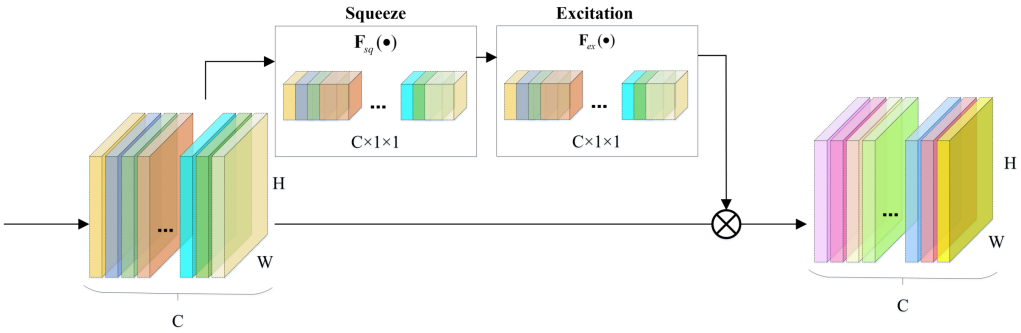

Figure 6. SE architecture. Squeeze: Global Information Embedding; Excitation: Adaptive Recalibration.

3.2. Long Short Term Memory Network Module

One variety of recurrent neural network is the LSTM (RNN). It works especially well for processing and forecasting occurrences with significant time series delays. In contrast to other RNNs, LSTM models use three gates and memory units to overcome gradient disappearance (see Figure 7). The forget gates play a role in determining which information from previous memory units to retain. The input gates make the determination of what data from the current input should be added to the memory unit as important. The output gates then regulate the model's following concealed state.

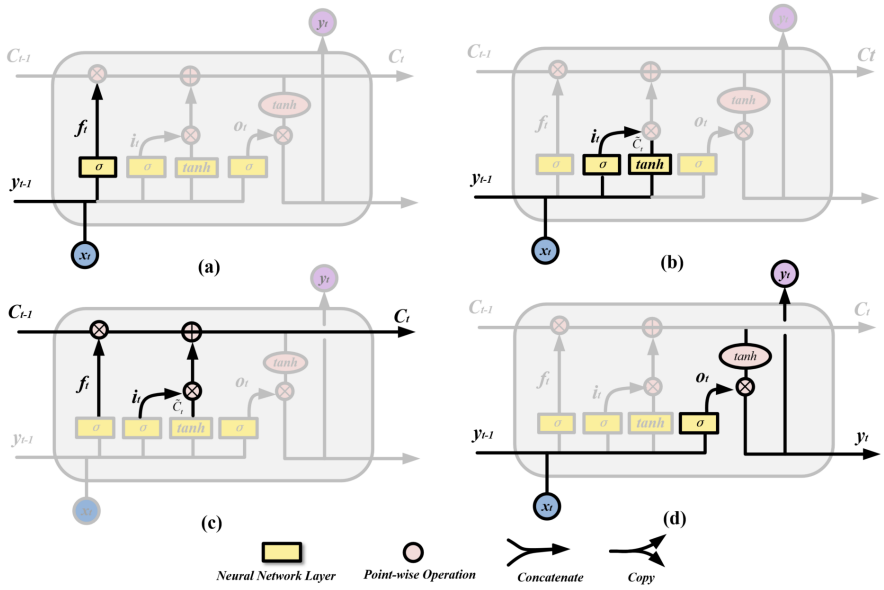

Figure 7. LSTM architecture. (**a**) Forget gate; (**b**) Input gate; (**c**) Memory unit; (**d**) Output gate.

(1) Forget gate: This step decides which information to discard, and its computation method is demonstrated in Equation (11).

$$S_{ft} = f_{\text{sigmod}}\left(\kappa_F \cdot [\varpi_{t-1}, \varphi_t] + \varrho_F\right) \tag{11}$$

Here, $[\varpi_{t-1}, \varphi_t]$ is the splicing of the output of the previous moment and the input of this moment. S_{ft} is the output of the forgetting gate.

(2) Input gate: This gate plays a crucial role in determining the extent to which new information should be incorporated.

$$S_{it} = f_{\text{sigmod}}\left(\kappa_I \cdot [\varpi_{t-1}, \varphi_t] + \varrho_I\right) \tag{12}$$

(3) Memory unit:

$$S_{mt} = \tanh(\kappa_M \cdot [\varpi_{t-1}, \varphi_t] + \varrho_M) \tag{13}$$

$$S_{mt} = S_{ft} * S_{mt-1} + S_{it} * S_{mt} \tag{14}$$

In the formula, the $*$ sign is used in multiplication operations between every element. The status of the cells in LSTM is changed from S_{mt-1} to S_{mt}.

(4) Output gate:

$$S_{ot} = f_{\text{sigmod}}\left(\kappa_g \cdot [\varpi_{t-1}, \varphi_t] + \varrho_g\right) \tag{15}$$

$$\Psi_t = S_{ot} * \tanh(S_{mt}) \tag{16}$$

Here, the result of the LSTM model is represented by Ψ_t .

3.3. Matrix-Based Fusion Module

After the above operations, time-frequency image features and time series features were extracted from closeness, period, and trend spectrum data. Next, features in the three types of input data need to be fused. In this paper, we chose matrix-based fusion, and assign different components to different weight matrices. Finally, the fused results will be used to predict the two-dimensional spectrum occupancy image through the tanh activation function.

4. Experiments and Results

4.1. Dataset Introduction

The dataset selected is the complex electromagnetic environment monitoring dataset of 5GXCAST [37] in the real environment of Turku [38], Finland. We selected 2017 and 2018 data for electromagnetic environment big data mining and spectrum sustainability risk prediction.

The measurement frequency band range, electromagnetic environment monitoring spectrum resolution, and time slot interval information of the original dataset are shown in Table 2.

Table 2. Raw measurement parameters of the dataset.

Band Number	Freq. Range	Resolution Bandwidth	Scan Interval (s)
1	30–130 MHz	78.125 kHz	10
2	130–800 MHz	39.0625 kHz	3
3	650–1200 MHz	39.0625 kHz	3
4	1200–3000 MHz	39.0625 kHz	3
5	3000–6000 MHz	78.125 kHz	3

In order to simplify the experiment, this paper mainly conducts big data mining and spectrum prediction for the spectrum with a frequency range of 2400–2700 MHz.

Before data mining of electromagnetic environment big data, to provide high-quality mining data raw elements, the electromagnetic environment data must be preprocessed. The data preprocessing steps are as follows.

- Missing and abnormal data handling: As there are no data missing in the original electromagnetic spectrum data, there is no need to complete the missing electromagnetic spectrum data. For the abnormal data values that seriously deviate from the overall data, this paper uses the average power spectral density value of the surrounding 3×3 area around it to replace it;
- Raw data downsampling: The original electromagnetic spectrum data has a very fine resolution, which makes the data values sparse, computation heavy and mining inefficient. On the other hand, since the original spectrum data is easy to mix with the electromagnetic environment noise during acquisition, the data with the original time domain resolution of 3 s are averaged every 20 time slots to remove equipment noise to a certain extent. The analyzed data have a 1 min time domain resolution as a result.

The processed data have a frequency precision of 976.5625 kHz because the power spectral densities of 25 nearby frequency points are averaged in the frequency domain.

4.2. Big Data Mining Results

4.2.1. Bottom Noise Mining Results

For this section, the 2400–2700 MHz spectrum data of one week in 2018 are selected as the experimental dataset. This frequency range includes the ISM (Industrial, Scientific, and Medical) service frequency band and the fixed communication frequency band, so there are obvious differences in the energy of different frequency points. The energy of occupied frequency points is much higher than that of idle frequency points.

Figure 8 (exported from MATLAB R2020b software) is a three-dimensional display of the original power spectral density data collected in this frequency band. The energy values in the 2400–2500 MHz and 2600–2700 MHz bands are high since this band is an ISM service band and fixed communication band, and the service is busy. The energy values in the 2500–2600 MHz band are low, because there is no fixed communication service in this band, and the frequency points are idle. Figure 9 (exported from MATLAB software) is a three-dimensional image of the electromagnetic environment bottom noise extracted by the adaptive threshold algorithm. The comparison between the two figures shows that the bottom noise mining algorithm designed by this paper can separate the signal from the bottom noise to a certain extent in the high-energy area while retaining the energy data in the low-energy area.

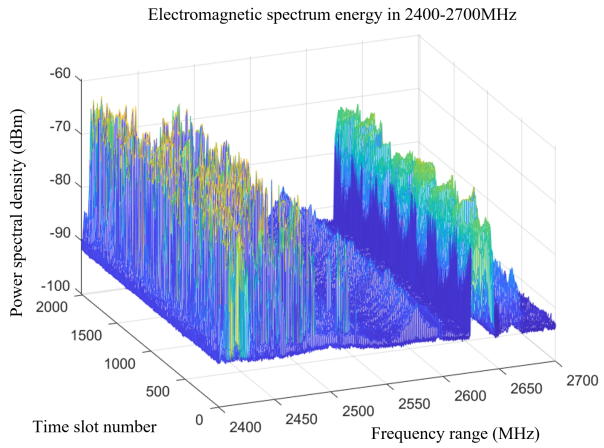

Figure 8. Spectrum energy in 2400–2700 MHz.

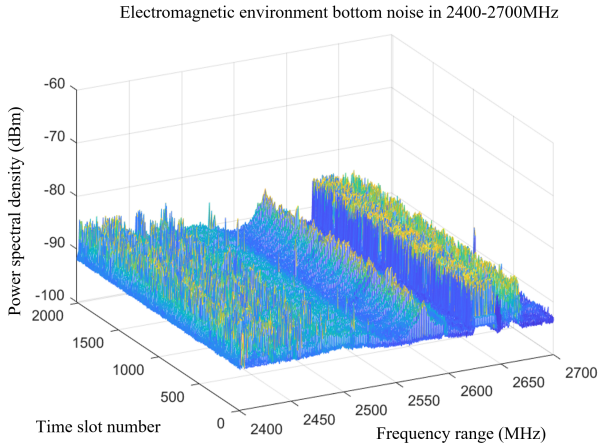

Figure 9. Bottom noise in 2400–2700 MHz.

4.2.2. Mining Results of Electromagnetic Environment Spectrum Occupancy

For this part, the 2500–2600 MHz spectrum data of eight days in 2017 and 2018 is selected as the experimental dataset. This frequency band range includes the ISM service frequency band and fixed communication frequency band. The evolution trend analysis of its spectrum occupancy shows a daily periodicity. Figure 10 (created in MATLAB software) shows the evolution of spectrum occupancy over eight days.

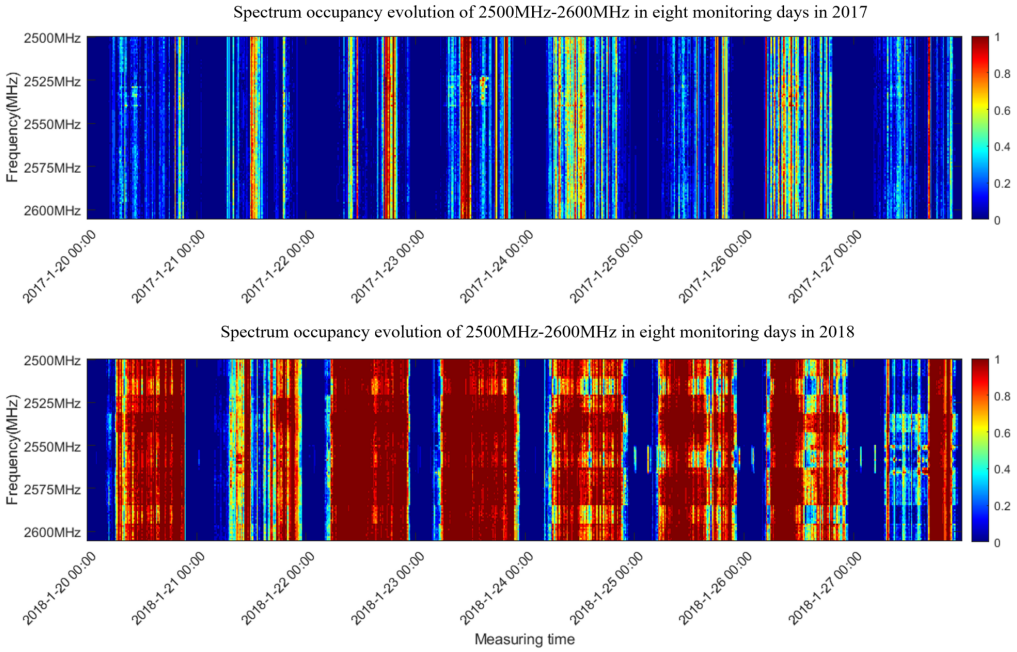

Figure 10. Spectrum occupancy evolution at 2500–2600 MHz over eight monitoring days in 2017 and 2018.

In Figure 10, the red area represents high spectrum occupancy and spectrum resource congestion, which means that the risk of spectrum resource sustainability is high; the blue area represents low spectrum occupancy and idle spectrum resources, which means that the sustainability risk of spectrum resources is low. The comparison of spectrum occupancy between 2017 and 2018 shows that, as time goes by, spectrum resources become crowded and busy due to the increase of frequency equipment. From the eight-day spectrum occupancy evolution in 2018, it can be seen that the red and blue spectrum occupancies intersect, that is, the busy and idle spectrum resources intersect, which is similar to the law of human activities. If robust and efficient prediction of spectrum occupancy can be achieved, spectrum resources can be reasonably scheduled to reduce the risk of spectrum resource sustainability.

4.3. Prediction of Spectrum Resource Sustainability Risk Based on TFBRL Network Experiment Results

4.3.1. Hyper-Parameters and Evaluation Indicators

The dataset was split into two non-overlapping parts, including training and test data, with a ratio of 7:3, in order to train the TFBRL model created in this article. The size of all convolution cores is 3 × 3. There are three residual convolution network units stacked, and the number of memory units of the LSTM network varies with the predicted time-frequency block size. The predicted multi-scale time-frequency occupancy image block size was set as $L \in \{4, 6, 8, ..., 44\}$, with a total of 20 spectrum image sizes. The batchsize was set to be 32 and epoch to 50.

In the evaluation process,the predicted time-frequency occupancy image block is compared with the real time-frequency occupancy image block. The TFBRL model is

evaluated using three commonly used regression task metrics, including MSE (mean square error), RMSE (root mean square error), and MAE (mean absolute error).

4.3.2. Comparison with Baselines

In this section, the prediction performance is presented compared to the LSTM, the Seq2seq, the Resnet(Residual network), the RNN, the CNN-LSTM and the TFBRL model.

- LSTM: The LSTM network used for modeling sequential data consists of two LSTM layers with hidden units, 32 and 16, respectively.
- Seq2seq: The Seq2seq network chooses a layer of the RNN network for its encoding layer and decoding layer, respectively. The RNN network has 32 hidden units.
- Resnet: The Resnet network with residual blocks using jump connection is easy to optimize, and can alleviate the problem of gradient disappearance.
- RNN: A layer of RNN network with short-term memory ability is used. The number of hidden units in the RNN network is 32.
- CNN-LSTM: The CNN-LSTM network not only has the feature extraction ability of CNN networks, but also has the long-term memory characteristics of the LSTM network. The model has three layers of two-dimensional convolutional neural networks with a $3 * 3$ convolution kernel.

4.3.3. Experimental Results

This software architecture for the experiment consists of Pytorch, a Python program created with Pycharm 2022.1.2 software. The Adam training algorithm was used to build the model on the GeForce RTX 3090 GPU from Nvidia. In order to be fair, six network models were the subject of several experiments in this paper. The experimental results are displayed in Tables 3 and 4, with the average of the results retained. Further, Figures 11–13 display how the predicted picture size affected the TFBRL network's and the baseline networks' prediction performance. To measure the network model's prediction performance from various angles, three distinct evaluation indicators were used.

Table 3. The baselines and the designed model's average prediction error.

Network	MSE	RMSE	MAE
RNN	0.30286	0.51829	0.42873
LSTM	0.33994	0.53536	0.45775
CNNLSTM	0.31717	0.52560	0.44731
Seq2seq	0.30583	0.52100	0.43084
Resnet	0.24220	0.46202	0.38154
TFBRL	0.16623	0.38808	0.33172

Table 4. Average predicted performance improvement percentage.

Network	Increase Percentage of MSE	Increase Percentage of RMSE	Increase Percentage of MAE
RNN	45.11%	25.12%	22.63%
LSTM	51.10%	27.51%	27.53%
CNNLSTM	47.59%	26.17%	25.84%
Seq2seq	45.65%	25.51%	23.01%
Resnet	31.37%	16.00%	13.06%
TFBRL	0.00%	0.00%	0.00%

Table 3 shows a comparison of the prediction performance between the TFBRL model and the baseline networks. The error value in the table is the average of the prediction error of time-frequency image blocks at various scales. Apparently, the TFBRL designed in this paper has the best prediction performance with the minimum prediction error value. Table 4 shows the average improvement percentage of TFBRL network prediction performance. The table shows that the TFBRL outperforms baseline networks to different degrees, and Table 4 shows average improvements on MSE, RMSE, and MAE of 31.37%, 16.00%, and 13.06%, respectively, over the best baseline.

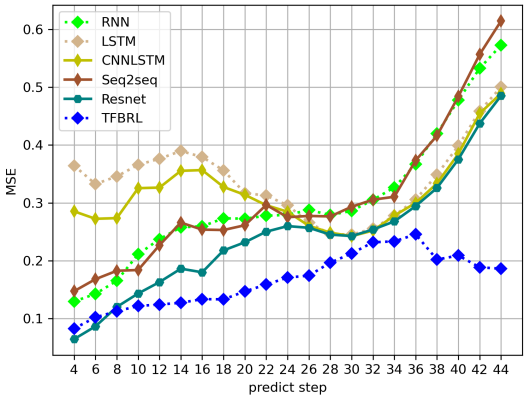

Figure 11. MSE vs. Length of predict step.

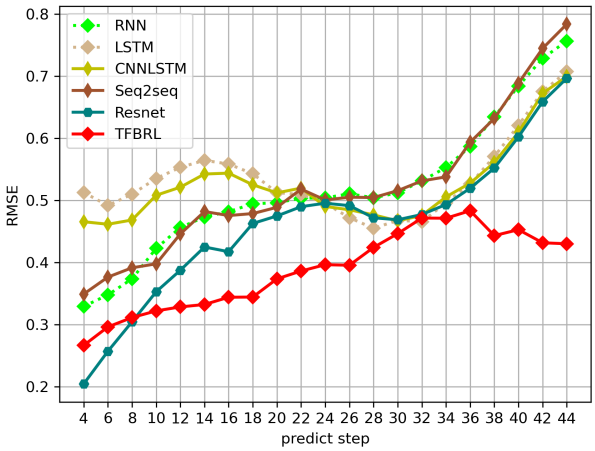

Figure 12. RMSE vs. Length of predict step.

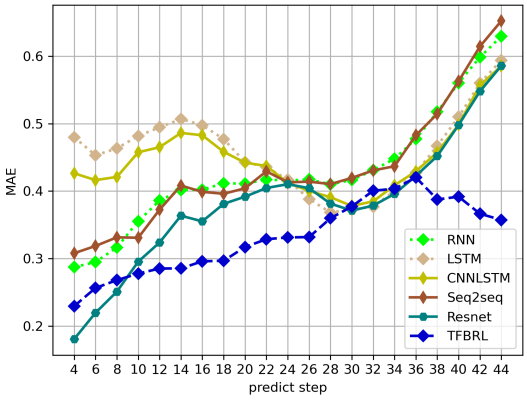

Figure 13. MAE vs. Length of predict step.

Figures 11–13 show the MSE RMSE and MAE values of network prediction errors of the TFBRL network and other baseline networks under different prediction steps. The different prediction steps represent the size of multiscale time-frequency occupancy image blocks.

Overall, the predictive performance of the network degrades as the block size of the predicted time-frequency image increases. By comparing the prediction performance of different networks, it can be found that the prediction performance of networks with residual structure is relatively more robust. This demonstrates that the residual structure can reduce the transmission of network spectral characteristics between network layers, lower the transmission of network spectral characteristics between network levels, and enhance prediction performance. The TFBRL network prediction developed in this

article is more precise and stable when compared to the prediction performance of other baseline networks.

4.3.4. Analysis of Parameter Sensitivity

The TFBRL is superior to the traditional shallow single network model since it incorporates the residual module and the memory characteristics of the LSTM network. We then compare the TFBRL model and its variations, which are indicated as follows, using the MSE, RMSE, and MAE metrics:

- TFBRL: Model described in this paper;
- TFBRL-rSE: The TFBRL network without SE attention.

Figures 14–16 show the MSE RMSE and MAE values of network prediction errors of TFBRL and TFBRL without SE attention. The figures clearly show that the evaluation values of the three prediction error indicators indicate superior performance of the model designed in this paper compared to its variants. Although the performances of the TFBRL model and TFBRL model without attention mechanism fluctuate under different prediction steps, in general, the TFBRL model has lower prediction error and better prediction performance.

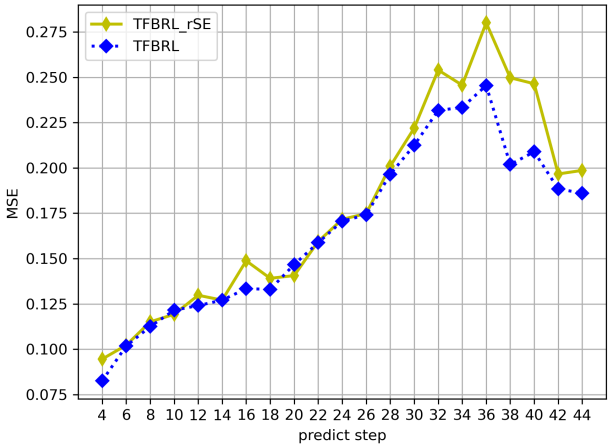

Figure 14. MSE vs. Length of predict step for the TFBRL and the TFBRL-rSE.

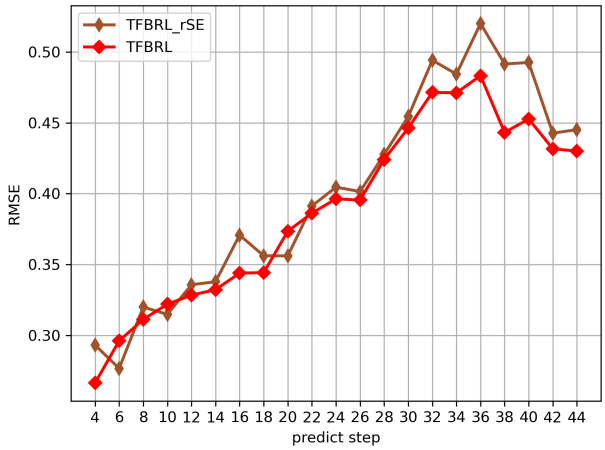

Figure 15. RMSE vs. Length of predict step for the TFBRL and the TFBRL-rSE.

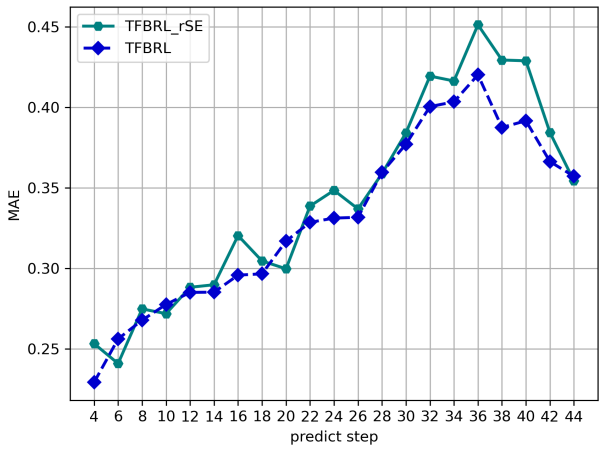

Figure 16. MAE vs. Length of predict step for the TFBRL and the TFBRL-rSE.

5. Discussion and Conclusions

A dynamic threshold algorithm was proposed in this paper to mine bottom noise and spectrum resource occupancy of electromagnetic environment big data. Compared with the traditional, manually defined fixed threshold, the dynamic threshold algorithm avoided the subjectivity inherent in manually selected thresholds.

A novel spectrum resources sustainable risk prediction algorithm based on the TFBRL network was presented in this paper. The proposed algorithm utilized the hourly time closeness, daily period, and annual trend as prior knowledge of spectrum resources for spectrum resource sustainability risk prediction. The TFBRL combines the feature extraction ability of a convolutional residual network and the time series analysis ability of an LSTM network, and fuses the channel attention mechanism to improve prediction performance. The simulation results for multiscale spectrum occupancy image prediction indicate that the proposed algorithm outperforms the baseline network model, showing an average improvement of 31.37%, 16.00%, and 13.06% over the best baseline model for the MSE, RMSE, and MAE metrics, respectively. Therefore, the TFBRL network is more suitable for two-dimensional spectrum occupancy image prediction.

In subsequent research, we can rely on the mining and prediction ability described here to guide specific frequency use behavior and spectrum management strategies, so as to enhance the sustainable development ability of spectrum resources and achieve reasonable allocation and scheduling of spectrum resources.

Author Contributions: S.L. contributed to the study design and wrote the manuscript drafts. Y.S. supervised the study and provided suggestions for the revision of the manuscript drafts. Y.H. provided suggestions for the revision of the manuscript drafts. O.A. contributed to the analysis of the data. A.T. provided some reviews on the manuscript. P.K.S. provided some reviews and suggestions for the revision of the manuscript drafts. All authors have read and agreed to the published version of the manuscript.

Funding: This research was funded by Researchers Supporting Project of King Saud University, Riyadh, Saudi Arabia (grant number RSPD2023R681), National Natural Science Foundation of China (General Program) (grant number 62201172).

Institutional Review Board Statement: Not applicable.

Informed Consent Statement: Not applicable.

Data Availability Statement: In this paper, the spectrum data used in the experiment comes from the open source spectrum monitoring project 5G-Xcast Open Spectrum data. The URL for open data is: https://zenodo.org/record/1300172 (accessed on 30 December 2022).

Conflicts of Interest: The authors declare that there is no conflict of interest regarding the publication of this paper.

Abbreviations

The following abbreviations are used in this manuscript:

TFBRL	Time-frequency block residual lstm
SE	Squeeze-and-excitation
AR	Autoregressive
SVR	Support vector regression
MLP	Multilayer perceptron
RNN	Recurrent neural network
TF^2AN	Temporal-frequency fusion attention network
CB-STSSN	Coud-based satellite and terrestrial spectrum shared networks
MTF^2N	Multi-channel temporal-frequency fusion network
PU	Primary spectrum user
SU	Secondary spectrum user
IIT	Illinois Institute of Technology
ISM	Industrial, Scientific, and Medical
Seq2seq	Sequence-to-sequence
Resnet	Residual network
CNN-LSTM	Convolutional neural network-Long short-term memory

References

1. Lin, Y.; Tu, Y.; Dou, Z.; Chen, L.; Mao, S. Contour Stella Image and Deep Learning for Signal Recognition in the Physical Layer. *IEEE Trans. Cogn. Commun. Netw.* **2020**, *7*, 34–46. [CrossRef]
2. Dong, Y.; Jiang, X.; Zhou, H.; Lin, Y.; Shi, Q. SR2CNN: Zero-Shot Learning for Signal Recognition. *IEEE Trans. Signal Process.* **2021**, *69*, 2316–2329. [CrossRef]
3. Tu, Y.; Lin, Y.; Zha, H.; Zhang, J.; Wang, Y.; Gui, G.; Mao, S. Large-scale real-world radio signal recognition with deep learning. *Chin. J. Aeronaut.* **2022**, *35*, 35–48. [CrossRef]
4. Hou, C.; Liu, G.; Tian, Q. Multi-signal Modulation Classification Using Sliding Window Detection and Complex Convolutional Network in Frequency Domain. *IEEE Internet Things J.* **2022**, *9*, 19438–19449. [CrossRef]
5. Shi, J.; Ge, B.; Liu, Y.; Shang, L. Data privacy security guaranteed network intrusion detection system based on federated learning. In Proceedings of the IEEE INFOCOM 2021—IEEE Conference on Computer Communications Workshops (INFOCOM WKSHPS), Vancouver, BC, Canada, 10–13 May 2021; pp. 1–6.
6. Guo, L.; Wang, M.; Lin, Y. Electromagnetic environment portrait based on big data mining. *Wirel. Commun. Mob. Comput.* **2021**, *2021*, 5563271. [CrossRef]
7. Zha, H.; Tian, Q.; Lin, Y. Real-world ADS-B signal recognition based on Radio Frequency fingerprinting. In Proceedings of the 2020 IEEE 28th International Conference on Network Protocols (ICNP), Madrid, Spain, 13–16 October 2020; pp. 1–6.
8. Bao, Z.; Lin, Y.; Zhang, S.; Li, Z.; Mao, S. Threat of Adversarial Attacks on DL-Based IoT Device Identification. *IEEE Internet Things J.* **2021**, *9*, 9012–9024. [CrossRef]
9. Tian, Q.; Zhang, S.; Mao, S.; Lin, Y. Adversarial attacks and defenses for digital communication signals identification. *Digit. Commun. Netw.* **2022**. [CrossRef]
10. Zhao, Y.; Ge, L.; Xie, H.; Bai, G.; Zhang, Z.; Wei, Q.; Lin, Y.; Liu, Y.; Zhou, F. ASTF: Visual Abstractions of Time-Varying Patterns in Radio Signals. *IEEE Trans. Vis. Comput. Graph.* **2022**, *29*, 214–224. [CrossRef]
11. Wang, M.; Lin, Y.; Tian, Q.; Si, G. Transfer Learning Promotes 6G Wireless Communications: Recent Advances and Future Challenges. *IEEE Trans. Reliab.* **2021**, *70*, 790–807. [CrossRef]
12. Wang, G.; Xiang, W.; Yuan, J. Outage Performance for Compute-and-Forward in Generalized Multi-Way Relay Channels. *IEEE Commun. Lett.* **2012**, *16*, 2099–2102. [CrossRef]
13. Long, H.; Xiang, W.; Wang, J.; Zhang, Y.; Wang, W. Cooperative jamming and power allocation with untrusty two-way relay nodes. *IET Commun.* **2014**, *8*, 2290–2297. [CrossRef]
14. Iranmanesh, R.; Pourahmad, A.; Faress, F.; Tutunchian, S.; Ariana, M.A.; Sadeqi, H.; Hosseini, S.; Alobaid, F.; Aghel, B. Introducing a Linear Empirical Correlation for Predicting the Mass Heat Capacity of Biomaterials. *Molecules* **2022**, *27*, 6540. [CrossRef]
15. Nabizadeh, M.; Jamali, S. Life and death of colloidal bonds control the rate-dependent rheology of gels. *Nat. Commun.* **2021**, *12*, 4274. [CrossRef]
16. Hosseini, S.; Taylan, O.; Abusurrah, M.; Akilan, T.; Nazemi, E.; Eftekhari-Zadeh, E.; Bano, F.; Roshani, G.H. Application of Wavelet Feature Extraction and Artificial Neural Networks for Improving the Performance of Gas–Liquid Two-Phase Flow Meters Used in Oil and Petrochemical Industries. *Polymers* **2021**, *13*, 3647. [CrossRef]
17. Mucchi, L.; Vuohtoniemi, R.; Virk, H.; Conti, A.; Hamalainen, M.; Iinatti, J.; Win, M.Z. Spectrum Occupancy and Interference Model Based on Network Experimentation in Hospital. *IEEE Trans. Wirel. Commun.* **2020**, *19*, 5666–5675. [CrossRef]

18. Wang, J.; Zha, H.; Fu, J. Evaluation of deep learning model in the field of electromagnetic signal recognition. In Proceedings of the IEEE INFOCOM 2022—IEEE Conference on Computer Communications Workshops (INFOCOM WKSHPS), New York, NY, USA, 2–5 May 2022; pp. 1–6.
19. Tandra, R.; Sahai, A.; Mishra, S.M. What is a Spectrum Hole and What Does it Take to Recognize One? *Proc. IEEE* **2009**, *97*, 824–848. [CrossRef]
20. Chen, Z.; Zhang, Y. Offshore Electromagnetic Spectrum Detection System Based on Self-Organizing Network. *IEEE Sens. J.* **2020**, *21*, 8650–8661. [CrossRef]
21. Chen, D.; Yin, S.; Zhang, Q.; Liu, M. Mining spectrum usage data: A large-scale spectrum measurement study. In Proceedings of the 15th Annual International Conference on Mobile Computing and Networking, MOBICOM 2009, Beijing, China, 20–25 September 2009; pp. 13–24.
22. Ding, G.; Wang, J.; Wu, Q.; Yao, Y.-D.; Li, R.; Zhang, H.; Zou, Y. On the limits of predictability in real-world radio spectrum state dynamics: from entropy theory to 5G spectrum sharing. *IEEE Commun. Mag.* **2015**, *53*, 178–183. [CrossRef]
23. Wen, Z.; Luo, T.; Xiang, W.; Ma, Y. Autoregressive spectrum hole prediction model for cognitive radio systems. In Proceedings of the ICC Workshops—2008 IEEE International Conference on Communications Workshops, Beijing, China, 19–23 May 2008; pp. 154–157.
24. Sapankevych, N.I.; Sankar, R. Time series prediction using support vector machines: A survey. *IEEE Comput. Intell. Mag.* **2009**, *4*, 24–38. [CrossRef]
25. Eltom, H.; Kandeepan, S.; Liang, Y.-C.; Evans, R.J. Cooperative Soft Fusion for HMM-Based Spectrum Occupancy Prediction. *IEEE Commun. Lett.* **2018**, *22*, 2144–2147. [CrossRef]
26. Yin, S.; Zhang, Q.; Zhang, E.; Yin, L.; Li, S. Statistical Modeling for Spectrum Usage Characterizing Wireless Fading Channels and Mobile Service Dynamics. *IEEE Trans. Veh. Technol.* **2013**, *62*, 3800–3812.
27. Tumuluru, V.K.; Wang, P.; Niyato, D. A neural network based spectrum prediction scheme for cognitive radio. In Proceedings of the 2010 IEEE International Conference on Communications, Cape Town, South Africa, 23–27 May 2020; pp. 1–5.
28. Shamsi, N.; Mousavinia, A.; Amirpour, H. A channel state prediction for multi-secondary users in a cognitive radio based on neural network. In Proceedings of the 2013 International Conference on Electronics, Computer and Computation (ICECCO), Almaty, Kazakhstan, 27–30 September 2013; pp. 200–203.
29. Yu, L.; Chen, J.; Ding, G. Spectrum prediction via long short term memory. In Proceedings of the 2017 3rd IEEE International Conference on Computer and Communications (ICCC), Chengdu, China, 13–16 December 2017; pp. 643–647.
30. Gao, Y.; Zhao, C.; Fu, N. Joint multi-channel multi-step spectrum prediction algorithm. In Proceedings of the 2021 IEEE 94th Vehicular Technology Conference (VTC2021-Fall), Online, 27 September–28 October 2021; pp. 1–5.
31. Zhao, Y.; Hong, Z.; Luo, Y.; Wang, G.; Pu, L. Prediction-Based Spectrum Management in Cognitive Radio Networks. *IEEE Syst. J.* **2017**, *12*, 3303–3314. [CrossRef]
32. Li, K.; Li, C.; Chen, J.; Zhang, Q.; Liu, Z.; He, S. Boost Spectrum Prediction with Temporal-Frequency Fusion Network via Transfer Learning. *IEEE Trans. Mob. Comput.* **2021**. [CrossRef]
33. Zhang, X.; Jia, M.; Gu, X.; Guo, Q. Intelligent spectrum management based on radio map for cloud-based satellite and terrestrial spectrum shared networks. *China Commun.* **2021**, *18*, 108–118. [CrossRef]
34. Li, S.; Sun, Y.; Zhang, H.; Zhang, Z.; Wang, M. MTF^{2}N: Multi-Channel Temporal-Frequency Fusion Network for Spectrum Prediction. In Proceedings of the GLOBECOM 2022-2022 IEEE Global Communications Conference, Rio de Janeiro, Brazil, 1–8 December 2022; pp. 4703–4709.
35. Ding, R.; Xu, M.; Zhou, F.; Wu, Q.; Hu, R.Q. RFML-Driven Spectrum Prediction: A Novel Model-Enabled Autoregressive Network. *IEEE Internet Things J.* **2022**, *9*, 18164–18165. [CrossRef]
36. Zhang, H.; Peng, S.; Zhang, J.; Lin, Y. Big Data Analysis and Prediction of Electromagnetic Spectrum Resources: A Graph Approach. *Sustainability* **2022**, *15*, 508. [CrossRef]
37. Bacchus, R.B.; Fertner, A.J.; Hood, C.S.; Roberson, D.A. Long-term, wide-band spectral monitoring in support of dynamic spectrum access networks at the IIT spectrum observatory. In Proceedings of the 2008 3rd IEEE Symposium on New Frontiers in Dynamic Spectrum Access Networks, Chicago, IL, USA, 14–17 October 2008; pp. 1–10.
38. Kalliovaara, J. 5G-Xcast Open Spectrum data 3/6. *Zenodo* **2018**. [CrossRef]